INTERNATIONAL JOURNAL OF PRECISION ENGINEERING AND MANUFACTURING-GREEN TECHNOLOGY Vol. 5, No. 2, pp. 255-260 APRIL 2018 / 255

REGULAR PAPER

DOI: 10.1007/s40684-018-0026-5
ISSN 2288-6206 (Print) / 2198-0810 (Online)

Efficient Microfluidic Power Generator Based on Interaction between DI Water and Hydrophobic-Channel Surface

Yong Whan Choi[1,2,*], Segeun Jang[1,2,*], Myung-Suk Chun[3], Sang Moon Kim[4,#], and Mansoo Choi[1,2]

1 Global Frontier Center for Multiscale Energy Systems, Seoul National University, 1, Gwanak-ro, Gwanak-gu, Seoul, 08826, Republic of Korea
2 Department of Mechanical and Aerospace Engineering, Seoul National University, 1, Gwanak-ro, Gwanak-gu, Seoul, 08826, Republic of Korea
3 Complex Fluids Laboratory, National Agenda Research Division, Korea Institute of Science and Technology, 5, Hwarang-ro 14-gil, Seongbuk-gu, Seoul, 02792, Republic of Korea
4 Department of Mechanical Engineering, Incheon National University, 119, Academy-ro, Yeonsu-gu, Incheon, 22012, Republic of Korea
Corresponding Author / E-mail: ksm7852@inu.ac.kr, TEL: +82-32-835-8096
ORCID: 0000-0002-2311-2211
*Yong Whan Choi and Segeun Jang contributed equally to this work

KEYWORDS: Streaming potential, Hydrophobic surface, Intrinsic charge, Microfluidics, Electrokinetics

The fabrication of power generators utilized by streaming potential has been attracting profound interests for various applications such as wearable healthcare and self-powered micro/nano systems. So far, streaming potential has been generated by a charged channel wall and accumulated counter-ions. However, this approach is assumed as no-slip boundary condition, while the slippery channel wall is critical for high efficiency. Herein, we demonstrate a microfluidic power generator based on streaming potential that can be intrinsically charged at a hydrophobic channel wall. This charging mechanism has higher values of charge density and slip boundary condition. We have achieved output voltage of ~2.7 V and streaming conductance density of ~1.23 A/m^2·bar with the channel that is ~2 μm high and ~3.5 μm wide. Our result is a promising step for obtaining low-cost, high efficient power-generators for micro/nano systems.

Manuscript received: February 17, 2017 / Revised: March 31, 2017 / Accepted: May 1, 2017

NOMENCLATURE

PG = Power-Generator
EDL = Electric double layer
DI = Deionized
PDMS = Polydimethylsiloxane
MEMS = Microelectromechanical systems
RIE = Reactive ion etching
C_4F_8 = Octafluorocyclobutane
VSFG = Vibrational sum-frequency generation
MD = Molecular dynamics

1. Introduction

The fabrication of self-powered micro/nano systems with sustainable, eco-friendly, and wireless operation properties is a key to realization of effective energy harvesting in the ambient environments.[1] Therefore, self-powered micro/nano systems have been extensively studied based on diverse mechanisms such as piezoelectricity,[1-3] triboelectricity,[4,5] pyroelectricity,[6,7] and streaming potential based power-generators (PGs).[8-16] Among the micro/nano PGs, the streaming potential based ones have the potentiality to be expanded to biomedical applications with the advantages of micro/nanofluidic systems which have been widely utilized in real-time monitoring biosensors,[17-19] biomedical diagnostics,[20] and DNA analysis.[21]

The streaming potential generated by the electrokinetic phenomena in micro/nanochannel occurs owing to the charge displacement in the electric double layer (EDL) caused by an external force shifting the liquid phase tangentially against the solid. It should be noted that studies on the streaming potential based PGs have been on the subjects of reducing the channel dimensions and modifying the surface property of the channel.[13,14,22] If the channel dimensions are reduced to the Debye screening length (i.e., EDL thickness), then the surface to volume ratio of

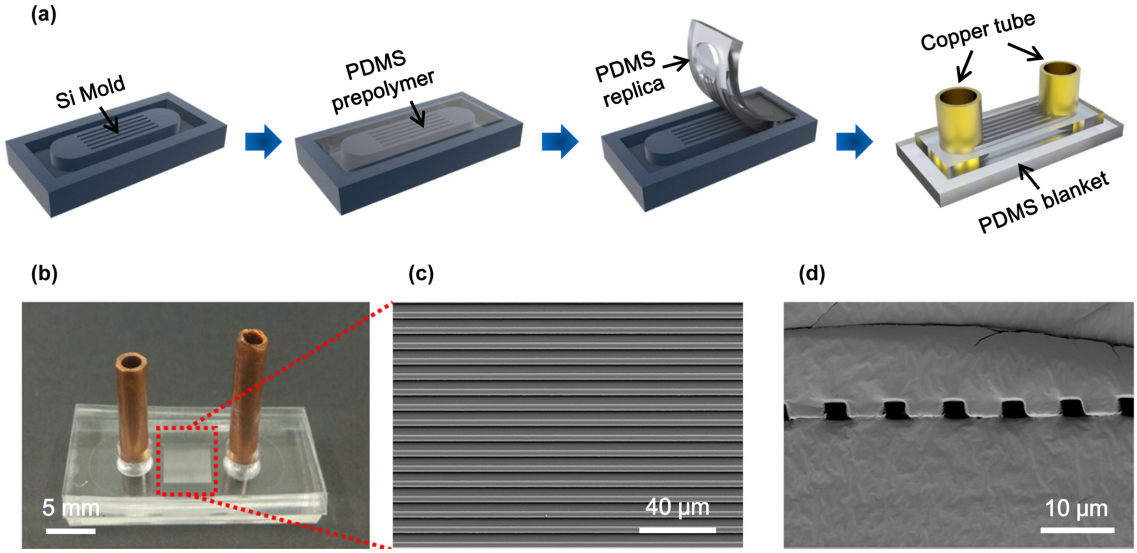

Fig. 1 (a) Schematic illustrations of fabrication process for microfluidic PG with soft lithography technology, (b) A digital camera image of as-fabricated microfluidic PG, (c) SEM images of the micro-line arrays on PDMS substrate, (d) Cross-Sectional SEM images of the micro-channel arrays inside the microfluidic PG

the channel system becomes exceptionally high and the utilization of high charge density becomes feasible. This leads to high efficiency of power conversion in the streaming potential based PGs.[10] While conventional micro/nanofluidic PGs have no-slip boundary condition at the fluid/solid channel interface, several studies investigated the benefit of the slippery channel surface. In the no-slip condition, highly concentrated ions near the channel walls are immobile as the working fluid flows. On the contrary, in the Navier's slip condition, highly concentrated ions within the range of the slip plane and the channel walls become mobile, which provides the enhanced efficiency of power conversion.[23,24] To the best of our knowledge, there have not been many studies pertaining to employing other charging mechanisms in streaming potential based PGs to generate currents and power.

In this paper, we report an eco-friendly and efficient microfluidic PGs based on the interaction between deionized (DI) water and hydrophobic-channel surface. We have used DI water as a working fluid and the hydrophobic polydimethylsiloxane (PDMS) as a solid channel in the streaming potential based microfluidic PG to make the interaction between the PDMS channel and DI water possess high charge density as well as inducing the slip boundary condition. By employing intrinsic charge generation at the interface between the DI water/hydrophobic surface and the slip-enhanced electrokinetic energy conversion, we have achieved output voltage of ~2.7 V and streaming conductance density of ~1.23 A/m^2·bar with the channel that is ~2 μm high and ~3.5 μm wide.

2. Experimental

The microfluidic PGs were fabricated through soft lithography and microelectromechanical systems (MEMS) technology.

2.1 Fabrications of Microfluidic Chip

Si master mold with micro-line patterns (Lines are 3.5 μm wide with a spacing of 4.5 μm; the entire patterned region is 5 mm in width and 4 mm in length) were fabricated by conventional photolithography technology and reactive ion etching (RIE) process. In order to compare the electrokinetic effect of microfluidic PGs with different channel heights, we made two micro-line patterned Si master molds with channels with heights of 2 and 6 μm. Next, post-surface treatment with octafluorocyclobutane (C_4F_8) gas was performed onto the Si master molds to reduce the surface energy and to better detach the PDMS mold.

Fig. 1(a) shows the fabrication process of the microfluidic PG. First, PDMS prepolymer was casted onto the surface-treated Si master mold and degassed in a vacuum chamber. Degassed PDMS prepolymer was thermally cured in an oven at 70°C for 2 hr. In this manner, the micro-line pattern on the Si master was replicated with PDMS material. Then, the PDMS replica was detached from the Si master mold and tailored in the size of 30 mm in length and 15 mm in width. The micro-line arrays were located in the center of the PDMS replica. The two ends of the PDMS replica had an empty semi-circle space that serves as a water resorvoir and has the electrodes located within. To make the inlet and outlet, two holes were punched at each end of the channel. Subsequently, the micro-line patterend PDMS replica was bonded with the flat PDMS blanket under an oxygen plasma treatment, and micro-channels were formed in the middle of the PDMS microfluidic chip. Since the oxygen plasma treatment made the PDMS surface temporarily hydrophilic, we placed the PDMS microfluidic chip into the oven at 120°C for two days so as to recover their inherent hydrophobic characteristics. We measured contact angles of the PDMS surfaces to confirm the recovery of hydrophobicity of PDMS which is treated with oxygen plasma. The contact angle of bare PDMS was ~108.3° and PDMS after 48 h in the oven at 120°C was ~104.5°. Finally, the microfluidic PG was made by inserting tubular Cu electrodes (outer diameter: 3 mm) into the two holes. These tubular shaped electrodes serve as both charge collector and fluid tubing. Fig. 1(b) shows a digital camera image of our prepared microfluidic PG.

2.2 Microchannel Characterization

The microchannel is located in the center of the device, and a maginfied scanning microscopy image (SEM) and a sectional SEM image are shown in Figs. 1(c) and 1(d), respectively. The microchannel array is uniform and well-defined over a large area with the channel with a width of ~3.5 μm and a height of ~2 μm, which consists of solely hydrophobic PDMS materials. The SEM image of the device with different channels with a height of ~6 μm is shown in the inset image of Fig. 4(b). Surface images of microchannel patterned PDMS mold and cross-sectional images of microfluidic PGs were obtained by using field-emission scanning electron microscope (FE-SEM; Carl Zeiss Auriga).

2.3 Electric Power Measurements

Ethanol was injected into each reservoir of the fabricated microfluidic PG by using syringe to make a pathway of water inside the hydrophobic channel. Ethanol in the reservoir was substituted into water and pressure was applied to the channel to remove the ethanol remained inside. The water was driven by applying a nitrogen gas pressure difference by using microfluidic flow control system (Fluigent, FCS-EZ,). The resulting streaming potential/current was measured with a picoammeter (Keithley Instruments, 6517A) through Cu electrodes.

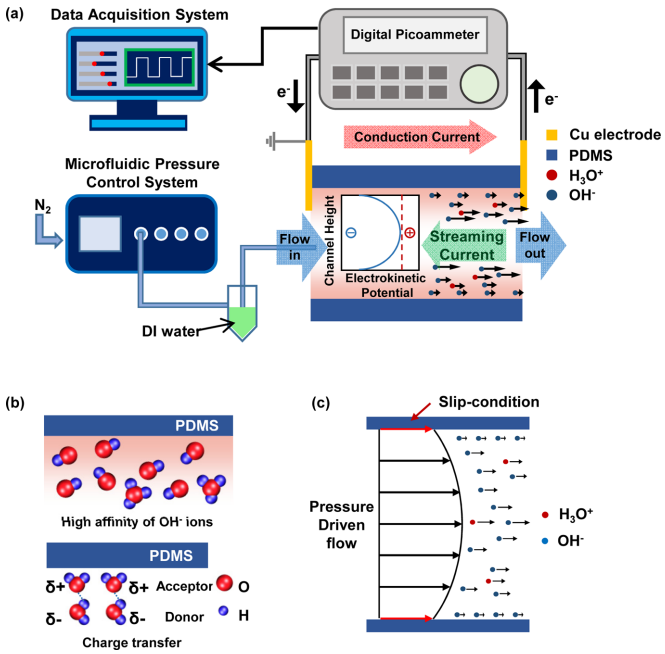

Fig. 2 (a) The illustration of our microfluidic PG system, and schematics of (b) charging mechanism at the interface between DI water and hydrophobic surface, (c) Slip-Enhanced electrokinetic effects

3. Results and Discussions

3.1 Principles of Intrinsic Charge Generation and Streaming Potential/Current

Fig. 2(a) shows the schematic illustrations of streaming potential/current. We applied a hydraulic pressure difference along the channel length by using microfluidic pressure control system (Fluigent, MFCS-EZ). Electrically neutral working fluids have an electrical charge distribution at the interface between the liquid and solid surface. This region is known as the EDL, which causes various electrokinetic phenomena such as electrophoresis, electro-osmosis, and streaming potential/current. Instead of the charged channel wall and the accumulated counter-ions, the DI water itself has been negatively charged at the water/hydrophobic interface. If the channel height reaches EDL thickness or becomes narrower, the EDLs are overlapped while negative ions become dominating charge carriers.[16] Therefore, the pressure-driven flow could carry a net negative charge. It induces both a potential difference and advection current, which are called streaming potential and streaming current. Fig. 2(b) demonstrates the schematic illustrations of EDL at the DI water/PDMS interface. Although hydrophobic materials such as PDMS are considered chemically inert and thus are not considered to have charge-generating groups,[25] recent experimental studies that used zeta potential measurement, vibrational sum-frequency generation (VSFG) spectroscopy and molecular dynamics (MD) simulations have confirmed that water becomes negatively charged in contact with hydrophobic interfaces.[22,26-30] However, the charging mechanism at the water-hydrophobic interfaces is still a subject of controversy.

The proposed mechanism suggested by previous studies can be summarized as mainly two postulates: (a) The specific adsorption of hydroxide ions (OH^-) to hydrophobic layer is stronger than H^+ (or hydronium ions) and this results in negative surface charge (Fig. 2(b) top).[27-29] (b) The charge transfer between water molecules can also give rise to negative surface charge. Compared to the isotropic environment of the bulk water, the symmetry of water molecules (e.g. tetrahedral arrangement) is broken at the water/hydrophobic interface. The truncation of hydrogen bonds results in imbalanced donating and accepting hydrogen bonds, which causes the hydrogen bond acceptor to be positively charged and the hydrogen bond donor to be negatively charged due to the electron density shift from the lone pair on the accepting oxygen to the donating water molecule (Fig. 2(b) bottom). This imbalance in donating and accepting hydrogen bonds induces a local excess negative charge in the water at ~0.5 nm from the Gibbs dividing surface (cf. this depth is close to the location of the slip plane for electrophoretic mobility measurements in water).[22,26,29,30] This negatively charged surface at the water/hydrophobic interface has also been confirmed by zeta potential measurement in previous reports.[19] Thanks to the intrinsic charge generation at the DI water/hydrophobic interface, streaming potential/current can be generated in our microfluidic PGs.

Hydrophobic property of PDMS channel allows to give rise to slip condition at the liquid/solid interface which induces the enhanced liquid flow velocity (shown in Fig. 2(c)).[31] It is assumed that the conventional PGs that use silica channel hold no-slip boundary condition and thus the fluid is stationary at the solid interface where the ion density is highly concentrated. Consequently, the capability of ionic transport is limited to these channel types. On the contrary, the hydrophobic surface can take advantage of slipping flow at the boundary, which decreases the fluidic impedance and increases the streaming conductance. Therefore, the slip condition of the

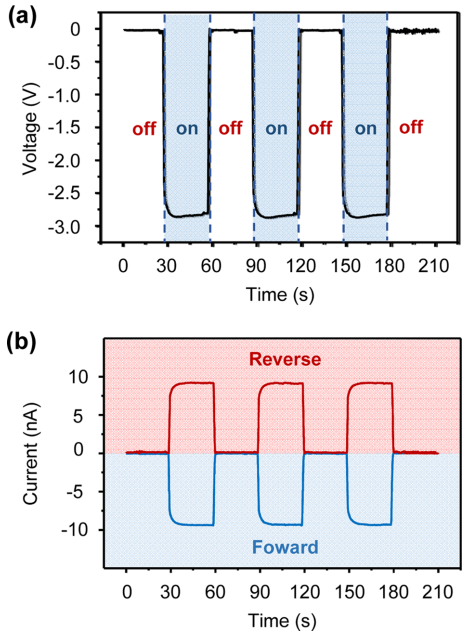

Fig. 3 Electrokinetic performances of the microfluidic PG, (a) Open-Circuit voltage, (b) Current outputs when flow direction is forward and backward

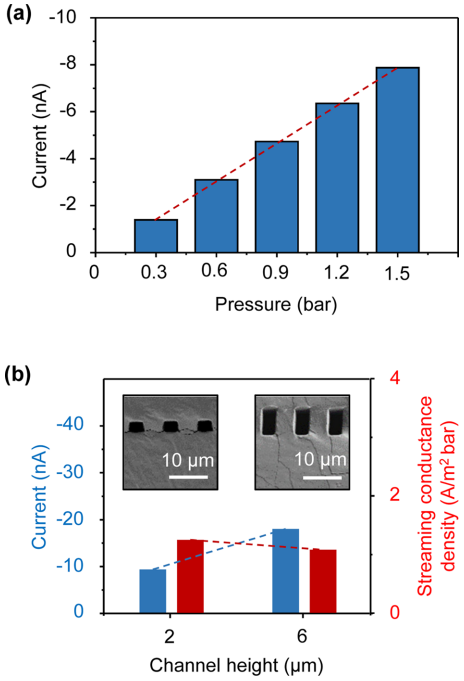

Fig. 4 (a) Output current versus input pressure, where the slope of fitting line indicates the streaming conductance, (b) Comparisons of current and streaming conductance density with variations of channel heights, where SEM images show the cross-sections of each channel with heights of 2 and 6 μm

hydrophobic surface should improve the electrokinetic energy conversion efficiency.

3.2 Electrokinetic Power Performances

Fig. 3 shows the electrical characteristics of the as-fabricated microfluidic PG. In this study, DI water was used as working fluid. Based on digital microfluidic pressure control system, the DI water runs through the hydrophobic micro-channel of the microfluidic PG. As mentioned earlier, the hydrophobic surface in contact with the DI water becomes negatively charged and therefore, the working fluid could carry a net electrical charge in EDL. When a pressure difference of 1.5 bar is applied, a constant open-circuit voltage output was measured as ~2.8 V. When the pressure difference was removed, the voltage outputs rapidly disappear and the same results were consistently observed by several repeated tests (shown in Fig. 3(a)). Under the same operating condition, the corresponding short-circuit current of ~8 nA was measured. Also, the steady outputs of the current are observed during on-off cycles. To confirm that the output currents are generated by microfluidic PG rather than the measurement system, a switching test was performed. As demonstrated in Fig. 3(b), when the direction of the working fluid was reversed, the same magnitude but opposite sign for the current outputs was observed. It confirms that the electrical outputs were generated by the microfluidic PG itself.

The dependence of the electrical outputs on the pressure difference was also investigated. The pressure difference was increased from 0 to 1.5 bar with a step of 0.3 bar. As shown in Fig. 4(a), the plot of the current output versus input pressure difference seems linear, which indicates that the microfluidic PG based on DI water and simple device configuration have the potentiality to be utilized as an active pressure sensor without any external power sources. Also, it is worthwhile to mention that the as-fabricated microfluidic PG shows the stable operating condition under varied pressure differences. From the linear fit of current variation by pressure, the slope is determined as ~5.4 nA/bar, which indicates the streaming conductance defined as $dQ/d\Delta V = dI/d\Delta p = S_{str}$,[14] where Q is the flow rate.

To investigate the effects of channel height in the microfluidic PG systems, electrical output voltage and streaming conductance were measured with channel heights of 2 and 6 μm, respectively (shown in Fig. 4(b)). The current outputs increase with increasing channel height, due to the increased flow rate of the device under the same pressure differences of 1.5 bar. It means that more energy is supplied to the system with the channel height of 6 μm (input energy is proportional to the multiplication of pressure difference and flow rate). To compare the efficiency of the device, we employed a streaming conductance density, which is streaming conductance divided by total channel cross-section area (~0.004 mm^2 for the channel height of 2 μm, ~0.013 mm^2 for the channel height of 6 μm). As a result, the streaming conductance density of the device with the channel height of 2 μm is higher than that with the channel height of 6 μm. For the channel height of 2 μm, streaming conductance density of ~1.23 A/m^2·bar is achieved. This is because the surface to volume ratio of the device with the channel height of 2 μm is 1.5 fold higher than that with the channel height of 6 μm and thus it could more effectively utilize the surface charge at the liquid/solid interface.

3.3 Comparison between DI Water and Tap Water

To verify the effectiveness of the DI water as a working fluid in the hydrophobic surfaces, the electrical outputs of the DI water (conductivity ~7 μS/cm, Human, Pure RO-360) versus tap water (conductivity ~209 μS/cm)[32] were measured and investigated (shown

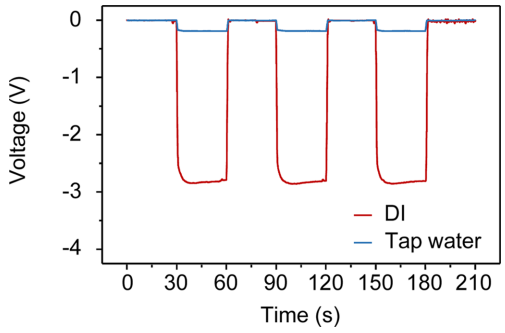

Fig. 5 Open-Circuit voltages of the DI water and Tap water

in Fig. 5). Since the ion concentration is proportional to the ionic conductivity and the EDL thickness is inversely proportional to the square root of the ion concentration, the EDL thickness of DI water is much thicker than that of tap water. When the tap water was utilized as a working fluid in the hydrophobic channel based microfluidic PG, the voltage outputs of ~0.2 V were observed. These values are quite low compared to those of DI water (~2.8 V). It indicates that the higher ion concentration in tap water than that in DI water results in compressing the EDL thickness and in decreasing net negative charge of fluid within the channel. This means that the diverse usage of these streaming potential based microfluidic PGs with intrinsic charging mechanism is possible and high streaming current/potential would be expected by using more purified water. These characteristics of the microfluidic PGs with intrinsic charging are distinguished from those of the conventional PGs performed by the deprotonation mechanism from the charged channel wall.

4. Conclusions

We report streaming potential based microfluidic PGs with the new charging mechanism for generation of intrinsic charge at the DI water/hydrophobic interface. The new charging mechanism possesses high surface charge density as well as inducing slip boundary condition. Based on the system, we achieved output voltage of ~2.7 V and streaming conductance density of ~1.23 A/m^2·bar with the channel height of ~2 μm. The experimental results showed the linear relationship between the applied pressure difference and the generated output current. We also elucidated the effect of the ion concentration on the streaming conductance by using DI water and tap water as working fluids. Our results suggest that the high surface to volume ratio would achieve higher efficiency, as the result of comparison of the channel heights of 2 and 6 μm shows. It would be further studied to achieve high energy conversion efficiency and total generated energy simultaneously by increasing working fluid flux.

ACKNOWLEDGEMENT

M. Choi acknowledges financial support by the Global Frontier R&D Program of the Center for Multiscale Energy Systems (No. 2012M3A6A7054855) funded from the National Research Foundation (NRF) of Korea. This work was also supported from the NRF of Korea by the Grant (No. 2016R1C1B1014564) provided to S. M. Kim and Mid-Career Researcher Program (No. 2015R1A2A1A15052979) provided to M.-S. Chun. On behalf of all authors, the corresponding author states that there is no conflict of interest.

REFERENCES

1. Zhong, J., Zhong, Q., Chen, G., Hu, B., Zhao, S., et al., "Surface Charge Self-Recovering Electret Film for Wearable Energy Conversion in a Harsh Environment," Energy & Environmental Science, Vol. 9, No. 10, pp. 3085-3091, 2016.
2. Wang, Z. L. and Song, J., "Piezoelectric Nanogenerators Based on Zinc Oxide Nanowire Arrays," Science, Vol. 312, No. 5771, pp. 242-246, 2006.
3. Kim, J. E., Kim, H., Yoon, H., Kim, Y. Y., and Youn, B. D., "An Energy Conversion Model for Cantilevered Piezoelectric Vibration Energy Harvesters Using Only Measurable Parameters," Int. J. Precis. Eng. Manuf.-Green Tech., Vol. 2, No. 1, pp. 51-57, 2015.
4. Bae, J., Lee, J., Kim, S., Ha, J., Lee, B.-S., et al., "Flutter-Driven Triboelectrification for Harvesting Wind Energy," Nature Communications, Vol. 5, Article No. 4929, 2014.
5. Zi, Y., Wang, J., Wang, S., Li, S., Wen, Z., et al., "Effective Energy Storage from a Triboelectric Nanogenerator," Nature Communications, Vol. 7, Article No. 10987, 2016.
6. Yang, Y., Jung, J. H., Yun, B. K., Zhang, F., Pradel, K. C., et al., "Flexible Pyroelectric Nanogenerators Using a Composite Structure of Lead-Free $KNbO_3$ Nanowires," Advanced Materials, Vol. 24, No. 39, pp. 5357-5362, 2012.
7. Nguyen, H., Navid, A., and Pilon, L., "Pyroelectric Energy Converter Using Co-Polymer P (VDF-TrFE) and Olsen Cycle for Waste Heat Energy Harvesting," Applied Thermal Engineering, Vol. 30, No. 14, pp. 2127-2137, 2010.
8. Siria, A., Poncharal, P., Biance, A.-L., Fulcrand, R., Blase, X., et al., "Giant Osmotic Energy Conversion Measured in a Single Transmembrane Boron Nitride Nanotube," Nature, Vol. 494, No. 7438, pp. 455-458, 2013.
9. Guo, W., Cheng, C., Wu, Y., Jiang, Y., Gao, J., et al., "Bio-Inspired Two-Dimensional Nanofluidic Generators Based on a Layered Graphene Hydrogel Membrane," Advanced Materials, Vol. 25, No. 42, pp. 6064-6068, 2013.
10. Haldrup, S., Catalano, J., Hansen, M. R., Wagner, M., Jensen, G. V., et al., "High Electrokinetic Energy Conversion Efficiency in Charged Nanoporous Nitrocellulose/Sulfonated Polystyrene Membranes," Nano Letters, Vol. 15, No. 2, pp. 1158-1165, 2015.
11. Chun, M.-S., Lee, T. S., and Choi, N. W., "Microfluidic Analysis of Electrokinetic Streaming Potential Induced by Microflows of Monovalent Electrolyte Solution," Journal of Micromechanics and Microengineering, Vol. 15, No. 4, pp. 710-719, 2005.

12. Chun, M.-S., Shim, M. S., and Choi, N. W., "Fabrication and Validation of a Multi-Channel Type Microfluidic Chip for Electrokinetic Streaming Potential Devices," Lab on a Chip, Vol. 6, No. 2, pp. 302-309, 2006.

13. Van der Heyden, F. H., Bonthuis, D. J., Stein, D., Meyer, C., and Dekker, C., "Electrokinetic Energy Conversion Efficiency in Nanofluidic Channels," Nano Letters, Vol. 6, No. 10, pp. 2232-2237, 2006.

14. Van Der Heyden, F. H., Bonthuis, D. J., Stein, D., Meyer, C., and Dekker, C., "Power Generation by Pressure-Driven Transport of Ions in Nanofluidic Channels," Nano Letters, Vol. 7, No. 4, pp. 1022-1025, 2007.

15. Van Der Heyden, F. H., Stein, D., and Dekker, C., "Streaming Currents in a Single Nanofluidic Channel," Physical Review Letters, Vol. 95, No. 11, Paper No. 116104, 2005.

16. Koltonow, A. R. and Huang, J., "Two-Dimensional Nanofluidics," Science, Vol. 351, No. 6280, pp. 1395-1396, 2016.

17. Zaytseva, N. V., Goral, V. N., Montagna, R. A., and Baeumner, A. J., "Development of a Microfluidic Biosensor Module for Pathogen Detection," Lab on a Chip, Vol. 5, No. 8, pp. 805-811, 2005.

18. Kurita, R., Hayashi, K., Fan, X., Yamamoto, K., Kato, T., et al., "Microfluidic Device Integrated with Pre-Reactor and Dual Enzyme-Modified Microelectrodes for Monitoring in Vivo Glucose and Lactate," Sensors and Actuators B: Chemical, Vol. 87, No. 2, pp. 296-303, 2002.

19. Kim, H. J., Jang, W. K., Kim, B. H., and Seo, Y. H., "Advancing Liquid Front Shape Control in Capillary Filling of Microchannel via Arrangement of Microposts for Microfluidic Biomedical Sensors," Int. J. Precis. Eng. Manuf., Vol. 17, No. 1, pp. 59-63, 2016.

20. Yager, P., Edwards, T., Fu, E., Helton, K., Nelson, K., et al., "Microfluidic Diagnostic Technologies for Global Public Health," Nature, Vol. 442, No. 7101, pp. 412-418, 2006.

21. Sun, Y. and Kwok, Y. C., "Polymeric Microfluidic System for DNA Analysis," Analytica Chimica Acta, Vol. 556, No. 1, pp. 80-96, 2006.

22. Lin, C.-H., Ferguson, G. S., and Chaudhury, M. K., "Electrokinetics of Polar Liquids in Contact with Nonpolar Surfaces," Langmuir, Vol. 29, No. 25, pp. 7793-7801, 2013.

23. Yang, J. and Kwok, D. Y., "Microfluid Flow in Circular Microchannel with Electrokinetic Effect and Navier's Slip Condition," Langmuir, Vol. 19, No. 4, pp. 1047-1053, 2003.

24. Ren, Y. and Stein, D., "Slip-Enhanced Electrokinetic Energy Conversion in Nanofluidic Channels," Nanotechnology, Vol. 19, No. 19, Paper No. 195707, 2008.

25. Tandon, V., Bhagavatula, S. K., Nelson, W. C., and Kirby, B. J., "Zeta Potential and Electroosmotic Mobility in Microfluidic Devices Fabricated from Hydrophobic Polymers: 1. The Origins of Charge," Electrophoresis, Vol. 29, No. 5, pp. 1092-1101, 2008.

26. Vacha, R., Marsalek, O., Willard, A. P., Bonthuis, D. J., Netz, R. R., et al., "Charge Transfer between Water Molecules as the Possible Origin of the Observed Charging at the Surface of Pure Water," The Journal of Physical Chemistry Letters, Vol. 3, No. 1, pp. 107-111, 2011.

27. Tian, C. and Shen, Y., "Structure and Charging of Hydrophobic Material/Water Interfaces Studied by Phase-Sensitive Sum-Frequency Vibrational Spectroscopy," Proceedings of the National Academy of Sciences, Vol. 106, No. 36, pp. 15148-15153, 2009.

28. Creux, P., Lachaise, J., Graciaa, A., and Beattie, J. K., "Specific Cation Effects at the Hydroxide-Charged Air/Water Interface," The Journal of Physical Chemistry C, Vol. 111, No. 9, pp. 3753-3755, 2007.

29. Strazdaite, S., Versluis, J., and Bakker, H. J., "Water Orientation at Hydrophobic Interfaces," The Journal of Chemical Physics, Vol. 143, No. 8, Paper No. 084708, 2015.

30. Vácha, R., Rick, S. W., Jungwirth, P., de Beer, A. G., de Aguiar, H. B., et al., "The Orientation and Charge of Water at the Hydrophobic Oil Droplet–Water Interface," Journal of the American Chemical Society, Vol. 133, No. 26, pp. 10204-10210, 2011.

31. Joseph, P. and Tabeling, P., "Direct Measurement of the Apparent Slip Length," Physical Review E, Vol. 71, No. 3, Paper No. 035303, 2005.

32. K Water, www.k-water.or.kr (Accessed 25 OCT 2017)